Correction of Random Surface Roughness on Colloidal Probes in Measuring Adhesion

ARTICLE *in* LANGMUIR · FEBRUARY 2007

Impact Factor: 4.46 · DOI: 10.1021/la0622828 · Source: PubMed

Correction of Random Surface Roughness on Colloidal Probes in Measuring Adhesion

Seungho Yang, Huan Zhang, and Stephen M. Hsu*

Materials Science and Engineering Laboratory, National Institute of Standards and Technology, Gaithersburg, Maryland 20899

Received August 2, 2006. In Final Form: October 24, 2006

Atomic force microscopes (AFM) are commonly used to measure adhesion at nanoscale between two surfaces. To avoid uncertainties in the contact areas between the tip and the surface, colloidal probes have been used for adhesion measurements. We measured adhesion between glass spheres and silicon (100) surface using colloidal probes of different radii under controlled conditions (relative humidity of <3%, temperature of 25 ± 1 °C). Results showed that the adhesion forces did not correlate with the radii of the spheres as suggested by elastic contact mechanics theories. Surface roughness and random surface features were found on the surfaces of the colloidal probes. We evaluated various roughness parameters, Rumpf and Rabinovich models, and a load-bearing area correction model in an attempt to correct for the roughness effects on adhesion, but the results were unsatisfactory. We developed a new multiscale contact model taking into account elastic as well as plastic deformation in a successive contacting mode. The new model was able to correct for most of the surface roughness features except for surface ridges with sharp angular features, limited by the spherical asperity assumption made in the model.

1. Introduction

Adhesion measurement at the micro- and nanoscales between two solid surfaces is receiving increased attention due to rapid deployment in devices. Micro- and nanoscale devices are being developed for applications in process control, sensing and actuation, biomedical intervention, transportation, aerospace, data storage, and many others. Adhesion and stiction are the dominant issues in these devices limiting reliability and durability. As the sizes of the components continue to decrease, accurate determination of the adhesive forces at nanoscale are needed for device design, materials selection, and performance.

Adhesion is generally measured by the amount of force necessary to separate two surfaces in contact. At nanoscale, mechanical loading is often not the overwhelming force as in the macroscale, and surface forces such as Van der Waals, electrostatic, and capillary/meniscus forces become significant in controlling the pull-off forces. For hydrophilic surfaces, hydrolysis reactions with surfaces often cause additional attractive force contributing to higher adhesion. For contacts of solid surfaces without adhesive agents, adhesion is proportional to the real area of contact. Therefore, perturbations to the contact area such as surface roughness, waviness, and contaminant particles would significantly affect the adhesion force. In addition, statistical surface roughness descriptions, proven successful at macroscale, may be inadequate to characterize a nanoscale contact area.

Atomic force microscopy (AFM) has been used extensively to measure adhesive forces between surfaces at nanoscale. Nanoadhesive forces come from two sources: contact interfacial forces and noncontact forces such as Van der Waals or electrostatic forces. Adhesion is typically measured by the pull-off force between the cantilever tip and the surface. The challenge in the measurement often lies with the determination of the real area of contact. For sharp tips, the surface roughness and high contact pressures may cause the tip to rotate and the surface to deform. Ducker[1] introduced the use of colloidal probe tips by attaching a sphere to the cantilever to measure adhesion. The spherical shape of the tip provides controlled contact pressure, symmetry, and mostly elastic contacts. The contact geometry permits the use of elastic contact mechanics analysis such as Johnson−Kendall−Roberts (JKR)[2] and Derjaguin−Muller−Toporov (DMT)[3] models for data reduction.

Using JKR and DMT models, for two spheres in contact, the pull-off force (F_{ad}) can be expressed as

$$F_{ad} = \frac{3}{2}\pi\gamma R \tag{1}$$

$$F_{ad} = 2\pi\gamma R \tag{2}$$

where γ is the work of adhesion between the contacting surfaces, and R is the equivalent radius of the contacting bodies and is defined by

$$\frac{1}{R} = \frac{1}{R_1} + \frac{1}{R_2} \tag{3}$$

where R_1 and R_2 are the radii of contacting bodies. From these equations, the pull-off forces should be proportional to the radii of the spherical probe tips. Indeed, researchers have reported that pull-off forces are proportional to the radii of the probes in their studies.[4,5]

The above equations assume that the spheres are symmetrical and smooth under fully elastic contact with one another. Fuller and Tabor,[6] however, suggested that roughness may affect the adhesion force as reflected by the pull-off force. They measured

* Corresponding author. stephen.hsu@nist.gov.

(1) Ducker, W. A.; Senden, T. J.; Pashley, R. M. *Nature (London)* **1991**, *353*, 239−241.
(2) Johnson, K. L.; Kendall, K.; Roberts, A. D. *Proc. R. Soc. London, Ser. A* **1971**, *324*, 301−313.
(3) Derjaguin, B. V.; Muller, V. M.; Toporov, Y. P. *J. Colloid Interface Sci.* **1975**, *67*, 314−326.
(4) Heim, L.-O.; Blum, J. *Phys. Rev. Lett.* **1999**, *83*, 3328−3331.
(5) Yoon, E. S.; Yang, S. H.; Han, H. G.; Kong, H. *Wear* **2003**, *254*, 974−980.
(6) Fuller, K. N. G.; Tabor, D. *Proc. R. Soc. London, Ser. A* **1975**, *345*, 327−342.

10.1021/la0622828
Published on Web 12/15/2006

the pull-off forces between an optically smooth rubber sphere and a hard−flat−smooth Perspex surface with varying degrees of roughness. Results showed that adhesion was significantly reduced by surface roughness, and they developed a model for adhesion of rough surfaces and allowed for elastic deformation of asperities using a statistical surface description of the asperity heights. Briscoe[7] conducted a systematic study of polyurethane on steel surfaces with controlled roughness and found that the adhesive peeling energy decreased as the roughness was increased. On the basis of these reports, surface roughness should affect the measured adhesive force, and this will interfere with the relation suggested by eqs 1−3. To investigate the effect of roughness on nanoscale contacts, Ando[8] used tips with varying radii and roughness in measuring adhesion in a 20−30% relative humidity environment and found that the pull-off forces were proportional to the tip radii. He suggested that the apparent insensitivity of the adhesive force to surface roughness was primarily due to the fact that water meniscus was always present in his contacts and the adhesion force was dominated by the capillary forces. So, under relatively humid conditions, surface roughness did not play a significant role.

Under relatively dry contact conditions, therefore, surface roughness should be a factor influencing the adhesion measurement. The degree of influence and how to correct for the roughness have not been well-defined. It is the aim of this study to examine the effect of surface roughness of colloidal probes on nanoadhesion. We have investigated the effect of surface roughness on adhesion measurement between glass beads of various radii and a flat silicon surface. The measurement of the contact surface roughness of a colloidal probe poses additional challenges. Since the total surface area is very small, surface roughness over the whole sphere may not be statistically uniform; therefore, the roughness of the contact area needs to be measured specifically at the place where contact is made. For determining the exact location of the contact spot on the colloidal probe, we adopted the reverse AFM imaging method developed by Neto and Craig[9] to identify the contact location by scanning the colloidal probe tip against a grating sample. Once the contact location of a glass sphere was determined, the surface is directly imaged by an AFM with a weak cantilever and a sharp tip to provide detailed three-dimensional surface topography. Using the digitized image, we compared various contact models to correct for the effect of roughness.

2. Experimental Procedures and Materials

Colloidal probes were prepared by gluing (Loctite, QuickSet Epoxy)[10] glass spheres (NIST, SRM 1003C) of various radii (3.3−17.4 μm) onto individual cantilevers (Veeco, NPS, nominal spring constants ~0.58 nN/nm).[10] A typical colloidal probe is shown in Figure 1. The colloidal probes were cleaned by high-purity ethanol in an ultrasonic bath for 1 min, followed by plasma cleaning (Harrick Plasma Cleaner, PDC-001) for 30 s before use. After cleaning, the bending stiffness of each probe was individually calibrated using the added mass technique.[11] The measured cantilever spring constants ranged from 0.19 to 0.34 nN/nm as shown in Table 1. The spring constants are significantly different from the supplied nominal value of 0.58 nN/nm. The radii of colloidal probes were measured by scanning a silicon grating sample (TGT01, NT−MDT),[10] and the results are shown in Table 1.

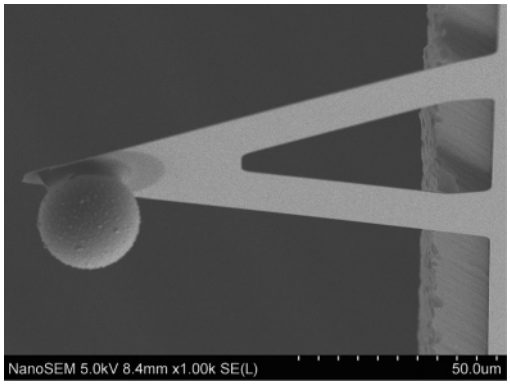

Figure 1. SEM image of the colloidal probe.

Table 1. Measured Radii and Bending Stiffness of Colloidal Probes (at a Level of Confidence of Approximately 95%)

radii of glued glass balls (μm)	bending stiffness in z direction of AFM cantilevers (nN/nm)
3.3 (±0.192)	0.19 (±0.012)
7.5 (±0.258)	0.29 (±0.020)
8.0 (±0.192)	0.30 (±0.012)
8.9 (±0.252)	0.33 (±0.024)
9.4 (±0.100)	0.34 (±0.012)
10.3 (±0.252)	0.28 (±0.012)
11.7 (±0.326)	0.27 (±0.012)
13.2 (±0.490)	0.28 (±0.012)
17.4 (±1.144)	0.25 (±0.020)

Silicon wafer (100) (Polishing Corporation of America)[10] samples were similarly cleaned in an ultrasonic bath with high-purity ethanol for 1 min and then in a plasma cleaner (Harrick Plasma Cleaner, PDC-001)[10] for 30 s before use.

The adhesion measurements were performed using an AFM (Multimode, Nanoscope IIIa, Veeco)[10] in a vibration-isolated temperature-controlled environment, as shown in Figure 2. Pull-off forces between the colloidal probes and the cleaned silicon (100) surface were measured under applied loads of 6 to 82 nN. The humidity was controlled by continuously feeding dry air into the AFM chamber to control the relative humidity at 3% (monitored by a digital hygrometer, Oakton, 35612, Thermohygrometer).[10] The silicon surface was electrically grounded by using a conducting silver paste (Three Bond, CNX-005)[10] to avoid electrostatic charge interference. A typical force−distance curve for the adhesion measurement is shown in Figure 3.

After the adhesion force measurement, the surface topographies of the silicon surface and the colloidal probes were scanned with a 0.06 nN/nm cantilever and a silicon nitride tip under contact mode. In order to scan only the contact area of the probe, a specially designed holder was fabricated to hold the colloidal probe at a specific inclined angle, and the contact surface was scanned,[12] as shown in Figure 4.

3. Experimental Results

Figure 5 shows the measured pull-off forces as a function of the probe radii. The experiments were conducted under various applied loads, from 6 to 82 nN for each probe tip. A minimum of three measurements were made at each load for each probe

(7) Briscoe, B. J.; Panesar, S. S. *J. Phys. D: Appl. Phys.* **1992**, *25*, A20−A27.
(8) Ando, Y.; Ino, J. *Wear* **1998**, *216*, 115−122.
(9) Neto, C.; Craig, V. S. J. *Langmuir* **2001**, *17*, 2097−2099.
(10) Certain instruments and materials are identified to adequately specify the experimental procedure. Such identification does not imply recommendation or endorsement by the National Institute of Standards and Technology, nor does it imply that the materials or instruments identified are necessarily the best available for the purpose.
(11) Cleveland, J.; Manne, S. *Rev. Sci. Instrum.* **1993**, *64*, 403−405.
(12) A new and direct method has been designed by the authors to measure the topography of colloidal probes at the spot where the contact is made. First, a colloidal probe is used to scan a grating sample (TGT1, NT-MDT) to identify the contact location. Second, the colloidal probe is mounted on an inclinable sample and scanned with an oxide-sharpened silicon nitride tip which was equipped at the end of a very compliant cantilever. The exact contact spot is located by changing the sample stage inclination angle θ. With this method, only a small scan size of 5 μm is needed for all the colloidal probes tested.

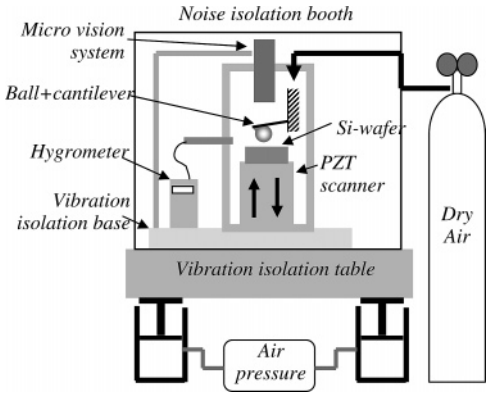

Figure 2. A schematic figure of AFM system used for adhesion measurement.

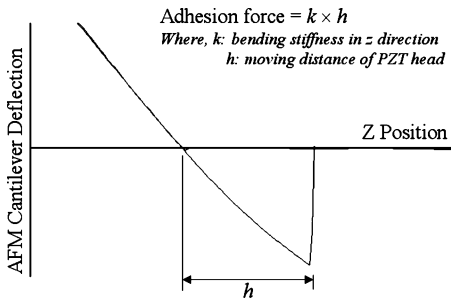

Figure 3. A typical force−distance plot and schematic illustration for adhesion force calculation.

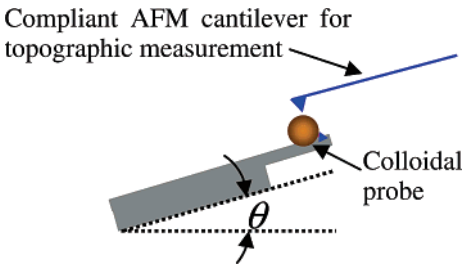

Figure 4. A schematic illustration on the method of measuring topography of colloidal probes.

tip. Repeated measurements were within 5% of the average value for each series. Varying the load did not change the pull-off force for each of the probe−surface contacts. The data in Figure 5 show that there is a lack of correlation of the pull-off forces with the radii of the colloidal probes. Similar plots of the measured adhesion forces as a function of the apparent areas of contact according to the models did not improve the correlation.

To understand why the adhesion forces did not correlate with the probe radii, we decided to examine the surface of the probes in detail. Figure 6 shows the three-dimensional surface topography of a group of colloidal probes (5 μm × 5 μm scan size, 512 × 512 resolution). We observed that these probe surfaces have two types of roughness: intrinsic baseline roughness and waviness of the polished sphere; and irregular protrusions/bumps randomly distributed on the surfaces. We surmised that the bumps were probably from particles stuck on the surface during the fabrication process. Since the spheres are basically silicon dioxide, tribochemistry and hydrolysis reactions would bond the glassy contamination particles onto the probe surface. Some of the random surface features are more than 50 times taller than the probe substrate surface roughness. The measured root-mean-

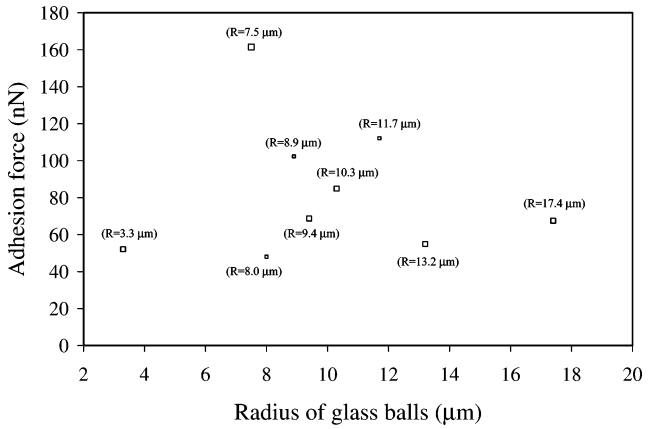

Figure 5. Measured adhesion forces plotted as a function of the radii of colloidal probes under the loads from 6 to 82 nN (size of symbol represents uncertainty (<5%) of data points).

square (rms) roughness values of these colloidal probes ranges from 20.6 to 45.4 nm, and they are tabulated in Table 2. The silicon surface used as a counter surface for the pull-off force measurements has an rms roughness of 0.5 nm; therefore, the colloidal probe roughness tends to dominate the contact condition.

3.1. Surface Roughness Correction. The effect of surface roughness on adhesion has been studied extensively in particle technology, adhesion science, and fundamental physics and chemistry. Rumpf[13] proposed a theoretical model based on contact of a single hemispherical asperity, centered at the surface and interacting with a much larger spherical particle along a line normal to the surface connecting their centers. Using the geometry and Derjaguin's[3] approximation for both contact and noncontact attractive forces related to Van der Waals interaction force, the following equation is obtained:

$$F_{ad} = \frac{H_0}{6z_0^2}\left[r + \frac{R}{(1 + r/z_0)^2}\right] \quad (4)$$

where H_0 is the Hamaker constant and its value can be approximately 1.31×10^{-19} J for the silica/silicon contact,[14,15] R is the radius of the particle, r is that of the asperity, and z_0 is the distance of the closest approach between surfaces. The value of z_0 is usually taken to be 0.3 nm, but different values have been suggested for a group of materials based on first principles.[16]

In studying the effects of nanoscale surface roughness on adhesion,[14,15] Rabinovich et al. proposed to link the average radius of hemispherical asperities to the measured rms roughness as follows:

$$r = 1.485\text{rms} \quad (5)$$

By substituting eq 5 into eq 4, the pull-off force can be related to the relative roughness which is defined by rms/R. Rabinovich's work found that this approach worked for nanometer-scale roughness. By using Rabinovich's model, Segeren et al.[17] also found that pull-off forces could be almost linearly related to the nanoscale rms surface roughness.

(13) Rumpf, H. *Particle Technology*; Chapman & Hall: London/New York, 1990.
(14) Rabinovich, Y. I.; Adler, J. J.; Ata, A.; Singh, R. K.; Moudgil, B. M. *J. Colloid Interface Sci.* **2000**, *232*, 10−16.
(15) Rabinovich, Y. I.; Adler, J. J.; Ata, A.; Singh, R. K.; Moudgil, B. M. *J. Colloid Interface Sci.* **2000**, *232*, 17−24.
(16) Yu, N.; Polycarpou, A. A. *J. Colloid Interface Sci.* **2004**, *278*, 428−435.
(17) Segeren, L. H. G. J.; Siebum, B.; Karssenberg, F. G.; Vanderburg, J. W. A.; Vancso, G. J. *J. Adhes. Sci. Technol.* **2002**, *16*, 793−828.

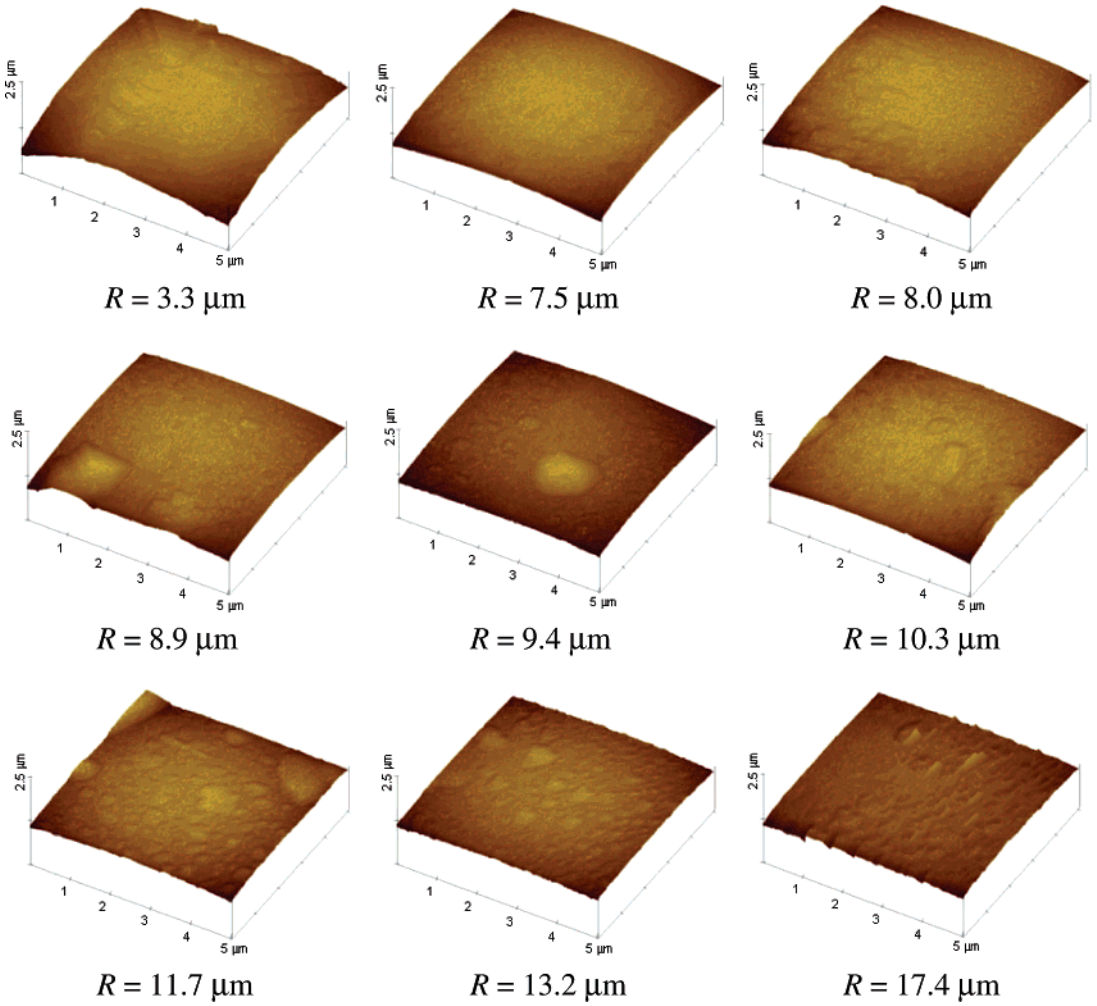

Figure 6. AFM topographies of the colloidal probe tip surfaces.

Table 2. Measured rms Roughness Values of Colloidal Probes[a 12]

radii of glued glass balls (μm)	rms[b] (nm)
3.3	42.5 (±7.8)
7.5	20.9 (±6.8)
8.0	20.6 (±15.4)
8.9	40.1 (±48.6)
9.4	45.4 (±51.2)
10.3	27.4 (±12.4)
11.7	31.8 (±7.8)
13.2	27.3 (±3.4)
17.4	40.0 (±5.2)

[a] The rms roughness of the Si wafer is 0.5 nm; thus, the roughness of colloidal probes dominates the contact. [b] Uncertainty range for AFM roughness measurement at this scale is about 10%. However, because of the combined size scales of baseline roughness and random features, the uncertainties calculated from normal procedure yield very large ranges.

Figure 7 presents the normalized measured pull-off force, $F_{ad}/(H_0R/6z_0^2)$, as a function of the relative roughness of the colloidal probes. For comparison, the theoretical prediction calculated by combining eqs 4 and 5 is also shown in the figure. The overall trend of increasing roughness with the dimensionless adhesion forces shows some improvement, but the predictions are much lower than the experimental results. This may be due to several factors. The Rabinovich model has a limitation in terms of difficulty in determining z_0 and types of roughness it can handle, since many random surface features are not amenable to statistical roughness treatment such as rms or rms/R.

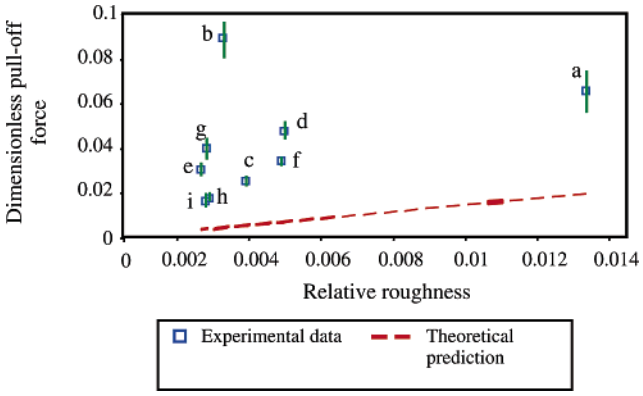

Figure 7. The dimensionless adhesion force $F_{ad}/(H_0R/6z_0^2)$ vs relative roughness rms/R (the size of error bar represents uncertainty (<5%) of data points): a, $R = 3.3$ μm; b, $R = 7.5$ μm; c, $R = 8.0$ μm; d, $R = 8.9$ μm; e, $R = 9.4$ μm; f, $R = 10.3$ μm; g, $R = 11.4$ μm; h, $R = 13.2$ μm; i, $R = 8.9$ μm.

If one examines the physical contact process between the colloidal probe with the random surface features with a flat surface, it is obvious that a sequential contact process would have to take place, i.e., the highest point touches the flat surface first, and as the forces begin to act, other part of the probe will come into contact. The rough surface of the colloidal probe would be progressively compressed by the flat until it reaches an equilibrium state between adhesion and resistance. This leads to the concept of load-bearing area determination which has been used in bearing technology.

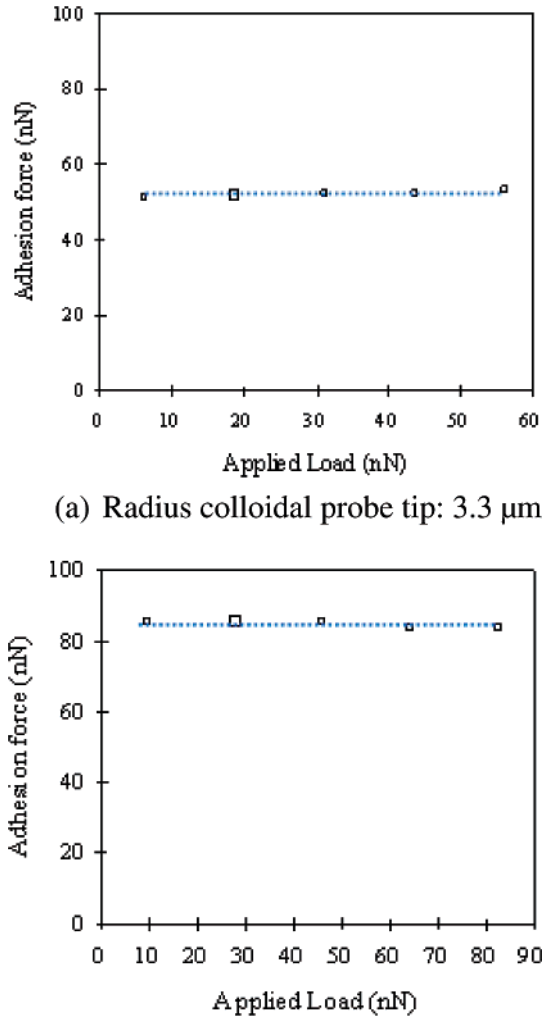

Figure 8. Typical examples of adhesion forces plotted as a function of applied loads (size of symbol represents uncertainty (<5%) of data points).

Table 3. Young's Modulus and Poisson's Ratio of Glass Ball and Si Wafer

	Young's modulus (GPa)	Poisson's ratio
glass ball	70[a]	0.25[a]
Si wafer	190[b]	0.42[b]

[a] ref 31. [b] ref 30.

3.2. Load-Bearing Area Correction. The basic concept of load-bearing area is that, when a rough surface is under compression, the asperities or the surface features will be compressed down to an equilibrium height at which the total compressive load is equal to the sum of the material reaction forces generated by the compressed asperities.

In our experiments, adhesion is measured by the pull-off force of the colloidal probe away from the silicon surface. The adhesive forces at the interface may be independent of the applied load[18,19] due to strong interfacial contact forces. This can be verified by conducting adhesion measurements under applied loads of 6 to 82 nN. Figure 8 shows typical pull-off forces measured with two probes of $R = 3.3$ μm and $R = 10.3$ μm, respectively. Other probes tested exhibit similar load independence, suggesting that,

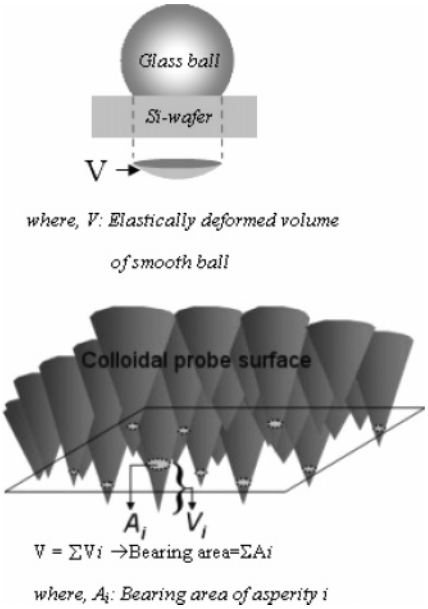

Figure 9. A schematic illustration of how the elastic deformation of glass ball was calculated.

once the contact is formed with the intrinsic colloidal probe surface roughness, the equilibrium adhesive force is constant within the load range applied.

The degree of elastic deformation may be characterized by a, the radius of contact. According to the JKR theory, the adhesion force at zero load leads to a radius of contact the same as that of the Hertzian contact under a load of the same amount as the adhesion force, i.e.,

$$a = \left(\frac{3NR}{4E'}\right)^{1/3} \tag{6}$$

where N is the normal force (the Hertzian contact load or adhesion force with no load applied), R the radius of glass sphere, and E' is the combined elastic modulus of glass sphere and silicon surface and is given by

$$E' = \left(\frac{1-\nu_1^2}{E_1} + \frac{1-\nu_2^2}{E_2}\right)^{-1} \tag{7}$$

where E_1 and E_2 are the Young's moduli of the colloidal probe and silicon respectively, and ν_1 and ν_2 are their Poisson's ratios. The values of these material parameters are listed in Table 3. For each of these probes, eq 6 is first used to calculate the nominal radius of contact with respect to the measured pull-off force. Since the nominal penetration depth of probe is much smaller than the probe radius, the corresponding material volume in elastic deformation can then be approximately determined as follows:[20]

$$V_e = \int_0^{\delta} 2\pi R(\delta - z)\, dz = \pi R\delta^2 \tag{8}$$

where δ is the nominal penetration depth

$$\delta = a^2/R \tag{9}$$

For a group of asperities on a rough surface, the volumetric elastic energy is stored in the form of compressed asperities. As illustrated in Figure 9, the overall compressive depth can be estimated when the total material volume estimated from the

(18) Zilberman, S.; Persson, B. N. J. *J. Chem. Phys.* **2003**, *118*, 6473−6480.
(19) Persson, B. N. J. *Phys. Rev. Lett.* **2002**, *89*, 245502.
(20) Johnson, K. L. *Contact Mechanics*; Cambridge University Press: Cambridge, 1985.

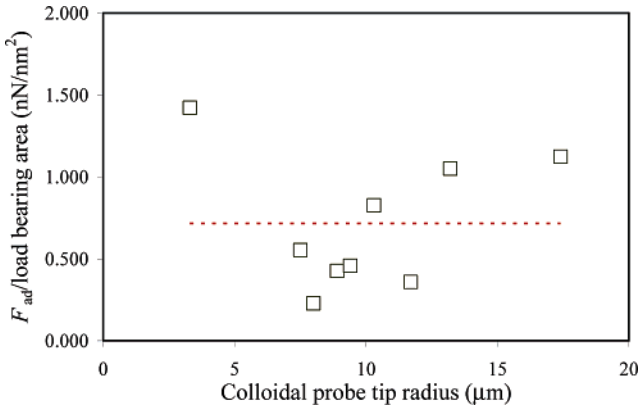

Figure 10. Normalized adhesion forces plotted as a function of colloidal probe radii (size of symbol represents uncertainty (<5%) of data points).

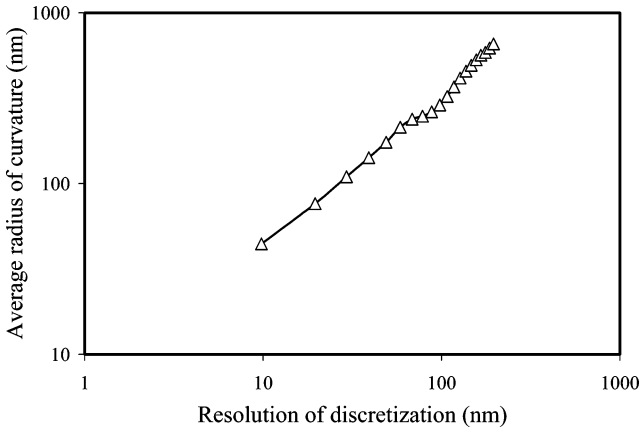

Figure 11. The average radius of curvature as a function of the discretization size (for the sphere of $R = 8.9$ μm).

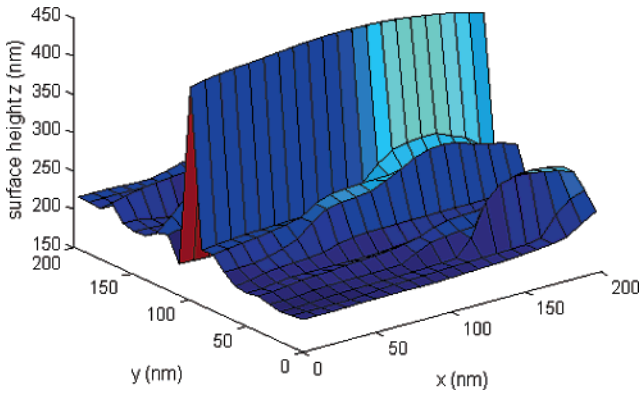

Figure 12. A small-angle wedge on the surface of the sphere with $R = 17.4$ μm.

measured topography at a depth of z is equal to the volume determined by eq 8. By compressing the highest-asperity peak successively at different levels of penetration depth, the final equilibrium compressed depth can be determined. This is the load-bearing area and is used to normalize the measured adhesion forces.

The procedure described above is applied to the group of colloidal probes with their digitized surface topography from AFM scans. If one takes the probe of $R = 3.3$ μm and that of $R = 10.3$ μm as two examples, with respect to their measured adhesion forces of $F_{ad} = 52.1$ nN and $F_{ad} = 84.9$ nN, the nominal penetration depths are $\delta = 5.26 \times 10^{-2}$ nm and $\delta = 4.98 \times 10^{-2}$ nm, respectively. The resulting elastic deformation volumes are $V_e = 28.7$ nm^3 and $V_e = 80.3$ nm^3, and the load-bearing areas of contact at the real penetration depths are 36.6 nm^2 and 103 nm^2.

Figure 10 presents the pull-off forces normalized by the load-bearing areas determined this way. If the roughness features are fully accounted for by the load-bearing areas, then the normalized pull-off forces should be a straight line against the probe radii. However, as shown in Figure 10, there is no straight-line relationship. This suggests that the surface roughness effects of the various colloidal probes are not being adequately corrected for by the use of the load-bearing areas.

4. Multiscale Contact Area Correction

The failure of the load-bearing area correction leads to a more in-depth examination of the nature of the contact at this scale. Chow[21] considered the issue when the size of particles varies over the entire range of scales, from nanometer to micrometers. He developed a theoretical model using the radius of curvature of asperities and incorporated them into a fractal description of surfaces and calculated the surface interaction energies. He found that surface forces could change by orders of magnitude depending on how surfaces in contact were influenced by the irregular fluctuations of rough surfaces at all length scales. The length scales and roughness exponent defined the distribution of asperities at contact at a particular scale. Bora et al.[22] examined the actual MEMS silicon surface and found multiscale surface roughness. Roughness at a smaller scale was shown to be similar to that at larger scales but with different length and height scaling factors, a property defined as self-affinity. They developed a multiscale contact model to describe the behavior of asperities at different discrete length scales. However, no experimental verification of the model was shown. Rimai et al.[23] studied micrometer and nanometer polystyrene and glass particles adhesion without mechanical loading on silicon and found that stress-induced strain for small particles on a surface could be very large, causing plastic deformation, and sometimes the particle could be engulfed into the substrate. These studies suggest that rough surface contact at nanoscale may involve multiscale behavior and scale-dependent deformation.

The multiscale nature of a rough surface can be examined by the dependence of the average radius of curvature on the scale sensitivity (measurement resolution at that scale) of the roughness measurement.[22,24] We determined the radii of curvature for the colloidal probes at different resolutions by finding the least-squares best-fit semi-ellipsoids to the data around distributed peaks or summits. Figure 11 shows the average radius of curvature obtained as a function of the resolution scale (discretization size) for the 8.0 μm radius probe. In this log−log plot, the radius of curvature can be seen to be almost linearly dependent on the discretization size. Similar power law dependence is also found for all other probes except for the 17.4 μm radius probe, which is characterized by multiple sharp wedges on the surface as shown in Figure 12.

It has been shown that a contact spot smaller than a critical contact area (subasperity) may undergo compressive loads larger

(21) Chow, T. S. *J. Phys.: Condens. Matter* **2003**, *15*, L83−L87.
(22) Bora, C. K.; Flater, E. E.; Street, M. D.; Redmond, J. M.; Starr, M. J.; Carpick, R. W.; Plesha, M. E. *Tribol. Lett.* **2005**, *19*, 37−48.
(23) Rimai, D. S.; Quesnel, D. J.; Busnaina, A. A. *Colloids Surf., A* **2000**, *165*, 3−10.
(24) Greenwood, J. A. Problems with surface roughness. In *Fundamentals of Friction, Macroscopic and Microscopic Processes*; Singer, I. L., Pollack, H. M., Eds.; Kluwer: Dordrecht, 1992; pp 57−76.

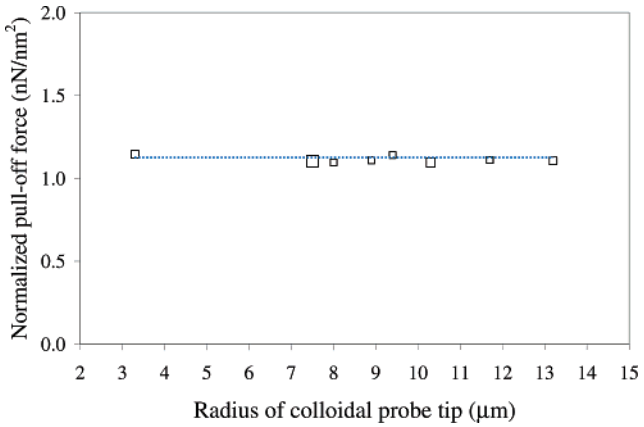

Figure 13. The measured pull-off forces normalized by the real area of contact vs the radii of glass spheres.

than its elastic limit, which introduces instability, and more asperities will come into play, and the larger contact may deform elastically.[25] Therefore, for random irregular surface roughness, the contact may undergo sequential multiscale contacting process migrating from one scale to another. This suggests that the subasperities or the sub-subasperities will come into contact first, and if the load instability ensures, the contact will expand to find other asperities to support the load. The likelihood for brittle materials being quasi-elastic and plastic at nanoscale has been shown by Lawn[26−28] and others. This process continues until the contact reaches a stable state where the global elastic deformation equilibrium is reached.

A multiscale sequential contact model based on the above discussion is developed and used to calculate the real areas of contact. In this model, the degree of compression of the asperities at the highest resolution (represented by the finest grid size) is examined first by calculating the surface contact pressure using a numerical method based on elastic contact models such as the following equations for independent asperities:

$$P_{\mathrm{m}}(\delta) = \frac{4E'}{3\pi}\left(\frac{\delta}{R_{\mathrm{c}}}\right)^{1/2} \tag{10}$$

$$A_{\mathrm{l}}(\delta) = \pi R_{\mathrm{c}}\delta \tag{11}$$

$$W_{\mathrm{l}}(\delta) = \frac{4E'}{3}(R_{\mathrm{c}}\delta)^{1/2}\,\delta \tag{12}$$

where E' is the reduced elastic modulus, δ the local interference, and R_{c} the asperity radius of curvature.

In the numerical solution algorithm, additional features are taken into consideration. When one asperity is compressed, at the same scale (same grid size), the surrounding asperities or summits are taken into the calculation, the degree of interlinking in terms of compressibility is defined as the influence coefficient.

With the colloidal probe surface topography digitized over a square (regular) grid at a grid size (scan resolution), the corresponding numerical solution routine to solve the elastic contact problem of all the asperities in contact at that scale is based on the following equations for calculating the displacements and pressure distribution at the grid points:[29]

$$g_{ij} = h_{ij} + u_{ij} - u_0 \text{ or } \mathbf{g} = \mathbf{h} + \mathbf{u} - u_0 \tag{13a}$$

$$u_{ij} = \Sigma_l\Sigma_k K_{ik,jl}\, p_{kl} \text{ or } \mathbf{u} = \mathbf{Ap} \tag{13b}$$

$$\Sigma_i\Sigma_j p_{ij} = P_0 \text{ or } \mathbf{q}^{\mathrm{t}}\mathbf{p} = P_0 \tag{13c}$$

where **h** is the gap between the surfaces just prior to any elastic deformation, **u** the composite surface displacement under the applied force F_0, **g** the gap after the deformation, **p** the interfacial pressure, u_0 is the rigid normal approach of one body to the other, P_0 is defined by $F_0 = \Delta x\Delta y P_0$, **q** is a vector of ones, and $K_{ik,jl}$ are the influence coefficients and **A** is the influence coefficient matrix. The above three groups of equations represent interface conformity conditions, elastic deformation equations, and equilibrium equation, respectively. The influence coefficients $K_{ik,jl}$ measure the normal displacement at the center of element (i, j) due to a unit pressure acting on element (k, l). They are determined by integrating the Boussinesq relationship between the concentrated point force and the surface normal deflection, i.e.,

$$K_{ik,jl} = \frac{1}{\pi E'}\int_{y_l-a_y/2}^{y_l+a_y/2}\int_{x_k-a_x/2}^{y_k+a_x/2}\frac{\mathrm{d}x\,\mathrm{d}y}{\sqrt{(x_i-x)^2+(y_j-x)^2}} \tag{14}$$

By solving eqs 13a−c, the surface contact area assuming that the deformation is elastic over the surface can be determined by summing up the areas of each element (i, j) with contact pressure P_{ij} larger than zero.

For most of these probes, the average pressures determined at the highest resolution are found much higher than the initial yield limit Y, ranging from 1.9 GPa to more than 20 GPa. This suggests that the subasperities in contact are unstable and will yield immediately to a larger contact area to cover more summits or asperities. For the group of colloidal probes examined, this procedure only fails for the 17.4 μm radius probe, which is characterized by sharp angle wedge features on the surface as shown in Figure 12. The failure is due to the intrinsic assumption that asperities are defined as semispherical shapes in our equations. For the remaining probes in this group, the final average contact pressure determined ranges between 1.10 and 1.14 GPa. For the 8.0 μm radius probe, the scale at which the contact becomes elastic is smaller than the highest resolution available and can be determined by searching downward with the topography refined by bilinear or bicubic interpolation. The resulting average contact pressure is also about 1.10 GPa. In summary, the areas of contact and the average pressures are determined for all the probes except for the 17.4 μm radius probe.

Figure 13 presents the pull-off forces normalized by the contact areas estimated from the multiscale numerical sequential contact model for the group of colloidal probes used in this study. In this figure, the 17.4 μm radius probe is not included, since we were not able to define its scale of equilibrium elastic contact. It can be seen that the normalized adhesion force (pull-off force divided by the contact area) falls on a horizontal straight line, suggesting that the adhesion force is a function of the "true contact areas" as predicted by the contact mechanics theory. The standard deviation of the normalized adhesion forces is about 1.7% of the average value (excluding the 17.4 μm radius probe). In comparison, the pull-off forces normalized by the load-bearing area have a standard deviation of about 57% of the corresponding

(25) Majumdar, A.; Bhushan, B. *ASME J. Tribol.* **1991**, *113*, 1−11.
(26) Lawn, B. R.; Padture, N. P.; Cai, H.; Guiberteau, F. *Science* **1994**, *263*, 1114−1116.
(27) Guiberteau, F.; Padture, N. P.; Lawn, B. R. *J. Am. Ceram. Soc.* **1994**, *77*, 1825−1831.
(28) Padture, N. P.; Lawn, B. R. *J. Am. Ceram. Soc.* **1994**, *77*, 2518−2522.
(29) Allwood, J. *ASME J. Tribol.* **2005**, *127*, 10−23.
(30) Peterson, K. E. *Proc. IEEE* **1982**, *70*, 420−457.
(31) Kharaz, A. H.; Gorham, D. A.; Salman, A. D. *Powder Technol.* **2001**, *120*, 281−291.

average value. In addition, another set of normalized pull-off forces is generated by correcting the dimensionless pull-off forces defined by $F_{ad}/(H_0R/6z_0^2)$ with the relative roughness, i.e., rms/*R*. The standard deviation of this group of results is about 70% of their average.

5. Conclusions

The dominating forces of adhesion between solid surfaces consist of van der Waals, electrostatic, and deformation forces.[2] For particles less than 1 μm in diameter, the electrostatic forces are not as important as the van der Waals forces.[21] In our study, the sample silicon surface is electrically grounded to avoid electrostatic charge force, and the humidity level is controlled so that the meniscus force influence is minimal. Our interest is in the use of colloidal probes to measure adhesion of solid−solid surfaces. We observed random surface features on the colloidal probe surfaces and the underlying surface roughness of the glass spheres we used for the probes. Attempts were then made to correct for the random protrusions and the background surface roughness with different models and calculation procedures. The accuracy and the effectiveness of the corrections were measured by the deviation of the normalized pull-off forces of different colloidal probes from a straight line.

We evaluated the basic Rumpf model, Rabinovich model, the load-bearing area model, and a multiscale contact numerical model. We found that, within the data availability, only the contact area estimated from the multiscale contact model provided an effective correction for the adhesion force measurements.

On the basis of the results described above, we can conclude the following:

(1) Surface roughness and the random surface features on colloidal probes interfere with the adhesion measurements using AFMs.

(2) Normal surface roughness parameters are insufficient in correcting the adhesion force measurement resulted from the probes.

(3) In comparison to the Rabinovich model, the load-bearing area calculated on the basis of volumetric elastic deformation is a better approximate correction for the probes studied in terms of the deviation normalized by the mean value.

(4) The surfaces of the colloidal probes have multiscale features, and the use of a multiscale contact model provides estimation of the contact areas which proves to be a more effective correction model for adhesion. However, its intrinsic assumption of spherical asperities makes it incapable of handling sharp ridges or geometries significantly different from spherical asperities.

Acknowledgment. The authors wish to acknowledge the help of Mr. Samuel N. Jones from the Precision Engineering Division, Manufacturing Engineering Laboratory at NIST for preparing the SEM images of the colloidal probes.

LA0622828